Electrochimica Acta 247 (2017) 942–948

Contents lists available at ScienceDirect

Electrochimica Acta

journal homepage: www.elsevier.com/locate/electacta

The Combined Influence of Gadolinium Doping and Non-stoichiometry on the Structural and Electrochemical Properties of Uranium Dioxide

Jandee Kim[a], Jeongmook Lee[a], Young-Sang Youn[a], Nazhen Liu[b], Jong-Goo Kim[a], Yeong-Keong Ha[a], Sang-Eun Bae[a,c], David W. Shoesmith[b,d,*], Jong-Yun Kim[a,c,**]

[a] Nuclear Chemistry Research Division, Korea Atomic Energy Research Institute, Daejeon 34057, Republic of Korea
[b] Department of Chemistry, Western University, London, Ontario N6A 5B7, Canada
[c] Radiochemistry & Nuclear Nonproliferation, University of Science and Technology, Daejeon 34113, Republic of Korea
[d] Surface Science Western, Western University, London, Ontario N6G 0J3, Canada

ARTICLE INFO

Article history:
Received 1 May 2017
Received in revised form 23 June 2017
Accepted 4 July 2017
Available online 11 July 2017

Keywords:
Urania
Oxygen stoichiometry
Gadolinium doping
Lattice structure
Cyclic voltammetry

ABSTRACT

The influence of Gd-doping level and oxygen stoichiometry on the structural properties and electrochemical reactivity of $U_{1-y}Gd_yO_{2\pm x}$ have been investigated. The stoichiometry of UO_2 matrices with different Gd contents was determined using the lattice parameter obtained by XRD. The extent of lattice contraction, defined by a contraction factor, was found to be dependent on the stoichiometry. The surface morphologies exhibited differences in grain size which varied with stoichiometry and its influence on the U atom diffusivity during fabrication. The differences in grain size and, hence, the density of grain boundaries was reflected in variations in electrical conductivity, with hyper-stoichiometric specimens with a low number of boundaries, yielding an increase in conductivity with increasing Gd content. Cyclic voltammetry showed that a variation in Gd content had only a minor influence on the electrochemical reactivity of stoichiometric $U_{1-y}Gd_yO_2$. By contrast, the reactivity of hypostoichiometric $U_{1-y}Gd_yO_{2-x}$ and hyperstoichiometric $U_{1-y}Gd_yO_{2+x}$ increased and decreased, respectively, with increasing Gd content. The formation of Gd-O_v clusters in hyperstoichiometric $U_{1-y}Gd_yO_{2+x}$ has a more marked influence on reactivity than the accompanying changes in grain size and electrical conductivity.

1. Introduction

The direct disposal of used nuclear fuel in deep geologic repositories has been under consideration internationally for many years. This requires the development of a source term to describe the radionuclide release processes on contact of the fuel with groundwater after container failure. This source term contains two contributions [1]; (i) the instant release fraction involving the instantaneous release of the cladding gap and grain boundary inventories; and (ii) the matrix dissolution fraction involving the slower release of radionuclides fixed within the matrix. The second fraction accounts for >90% of radionuclides and will be governed by the corrosion/dissolution of the UO_2 matrix.

Of key importance in determining fuel corrosion is the reactivity of the fuel matrix and how it is modified by in-reactor irradiation. The key changes expected to influence the reactivity of the fuel matrix are the presence of non-stoichiometry and fission product doping of the UO_2 matrix, especially by the trivalent rare earth ions (RE^{III}). While used fuel is expected to be close to stoichiometric UO_2, the stoichiometry can vary from hyper- to hypostoichiometry. Hyperstoichiometry (UO_{2+x}) has been shown to exert a major influence on UO_2 reactivity [2–4]. When close to stoichiometry, oxidation of the UO_2 matrix, the first step in the overall corrosion process, appears to be limited by the low mobility of interstitial oxygen ions within the matrix. At higher degrees of non-stoichiometry, the formation of defect clusters enhances interstitial mobility leading to increased oxidation rates. To date no concerted effort has been made to investigate the influence of hypostoichiometry on reactivity.

The influence of fission products, in particular RE^{III}, on the properties of UO_2 and its rate of oxidation in air have been extensively investigated [5–14]. By contrast studies on their influence on electrochemical reactivity have been much less

* Corresponding author at: Department of Chemistry, Western University, London, Ontario N6A 5B7, Canada.
** Corresponding author at: Nuclear Chemistry Research Division, Korea Atomic Energy Research Institute, Daejeon 34057, Republic of Korea.
E-mail addresses: dwshoesm@uwo.ca (D.W. Shoesmith), kjy@kaeri.re.kr (J.-Y. Kim).

http://dx.doi.org/10.1016/j.electacta.2017.07.023
0013-4686/

frequent [15,16]. Air oxidation studies show that oxidation of UO_2, or UO_2 doped with low concentrations of impurities, proceeds through U_3O_7 to the final product U_3O_8. By contrast, the oxidation of UO_2 doped with substantial amounts of rare earths or other fission products proceeds via U_4O_9, with the phase accommodating excess divalent oxygen ions (O^{II}) beyond the nominal stoichiometry of $UO_{2.25}$, with the further conversion to U_3O_8 being kinetically inhibited.

More recently [15–17] a similar suppression of the electrochemical reactivity of the UO_2 matrix by RE^{III}-doping has been demonstrated. This reduced reactivity was attributed to the formation of RE^{III}-O_V (O_V: oxygen vacancy) clusters accompanied by a contraction of the lattice. This combination of features leads to a reduction in the availability of the O_Vs required to accommodate O^{II} within the oxidized surface. These claims are consistent with the model calculations of Park and Olander [11] and the observations of Desgranges et al. [18]. These studies were conducted on extensively-doped with Gd (6 wt%) or Dy (12.9 wt %). More recent studies, conducted on $U_{1-y}Gd_yO_2$ ($0 \leq y \leq 0.1$) suggested a competition between an increase in reactivity at low doping levels, attributed to the creation of O_V, and a more marked decrease in reactivity at higher doping levels, due to defect clustering and the contraction of the lattice.

Despite these studies, the simultaneous influences of non-stoichiometry and RE^{III}-doping have not been investigated in any detail. In this study, we compare the characteristics and reactivity of Gd-doped UO_2 varying from hypostoichiometric, stoichiometric to hyperstoichiometric. Specimens were characterized using X-ray diffractometry (XRD), scanning electron microscopy (SEM), and by measurements of electrical conductivity. Their reactivity was determined using cyclic voltammetry.

2. Experimental

2.1. Pellet Preparation

Appropriate amounts of unirradiated UO_2 and Gd_2O_3 powder (99%, Aldrich, USA) were weighed and mixed in the proportions required to produce 0, 1, 3, 5 and 10 mol% Gd in UO_2. After grinding mechanically to a fine powder, green pellets were prepared by mechanical pressing at 300 MPa [12]. All pellets were *c.a.* 9 mm in diameter and <1 mm in height.

2.1.1. Sintering and Control of Stoichiometry

All green pellets were weighed before and after sintering to obtain a rough estimate of their oxygen content. Hypostoichiometric specimens were prepared by sintering in a furnace at 1700 °C in a reducing H_2 atmosphere. Stoichiometric and hyperstoichiometric specimens were prepared by sintering in a controlled CO/CO_2 atmosphere with a gas ratio in the range of 10 to 0.001, with the temperature and gas ratio chosen according to the Ellingham diagram [13,14]. To achieve hyperstoichiometry, a gas ratio of 0.001 and a high temperature is required. The conditions used to produce stoichiometric and hyperstoichiometric pellets are summarized in Table 1.

Table 1
The CO/CO_2 gas mixtures (to establish the required oxygen potential) and temperature (T) used to prepare hyperstoichiometric $U_{1-y}Gd_yO_{2+x}$ and stoichiometric $U_{1-y}Gd_yO_2$ pellets by oxidation of hypostoichiometric $U_{1-y}Gd_yO_{2-x}$ pellets.

y	$U_{1-y}Gd_yO_2$		$U_{1-y}Gd_yO_{2+x}$	
	CO/CO_2	T (°C)	CO/CO_2	T (°C)
0	10	800	0.1	1500
0.01	10	800	0.1	1500
0.03	10	800	0.1	1500
0.05	0.1	1200	0.001	1200
0.10	0.001	1200	0.001	1500

2.2. Electrical Conductivity Measurement for Solid Pellets

Electrical conductivities were calculated from specific resistivity (ohm·cm) measurements using the 4-point probe technique (HM21-Jandel Co., UK) at room temperature. All values are the average of three measurements on each sample.

2.3. Electrochemical Measurements

Electrodes were prepared by attaching the pellets to a steel shaft using an adhesive conductive silver paste (DOTITE, Japan) and then setting them into an epoxy resin, so that only the front face of the pellet was exposed. A Pt foil (99.99%, Aldrich) and a commercial saturated calomel electrode (SCE) (+0.242 V vs the standard hydrogen electrode) were used as the counter and reference electrodes, respectively. All electrochemical experiments were carried out using a potentiostat (CHI-600D, USA) to control applied potentials and record current responses. Electrodes were polished with 3000 grit SiC paper prior to an experiment and then cathodically cleaned at −1.2 V for 5 minutes before an experiment.

2.4. Chemicals and Solutions for Electrochemical Measurements

Solutions were prepared with deionized water with a resistivity (ρ) of 18.2 MΩ·cm purified using a Millipore Milli-Q plus unit to remove organic and inorganic impurities. Sodium carbonate (>98%, Aldrich) and sodium bicarbonate (99%, Aldrich) were added to a 0.1 M sodium chloride solution to yield a total carbonate concentration of 0.001 M. The pH was adjusted to *c.a.* 9.0 using a dilute sodium hydroxide solution (99.8%, Aldrich) and monitored with an Orion model 720A pH meter. Prior to an experiment, the solution was purged with Ar (>99%, Shincheon Gas, Korea) for 1 hour, and puring was maintained throughout the experiment.

2.5. Scanning Electron Microscopy (SEM) and X-ray Diffractometry (XRD)

SEM analyses were conducted with a JEOL JSM-6610LV microscope using a 20 keV electron accelerating voltage, with the working distance set to be 10 mm during image collection. XRD patterns were recorded using a Bruker AXS D8 Advanced X-ray Diffractometer using Cu K_α radiation at room temperature. XRD data were collected in the 2θ range from 20° to 120° using a 0.02° step size. The lattice parameters were calculated by Pawley's refinement process using the TOPAS (Version 4.2 Bruker AXS) analysis software.

3. Results

3.1. Lattice Structure

Fig. 1 shows values of the lattice parameter as a function of the Gd-doping level for $U_{1-y}Gd_yO_{2\pm x}$ specimens. The dashed line shows the calculated theoretical lattice parameter for the stoichiometric $U_{1-y}Gd_yO_2$ with increasing Gd content. The experimental data for the stoichiometric $U_{1-y}Gd_yO_2$ is well matched with this line as expected. The slope of this line is −0.0173, a reasonable contraction factor in agreement with published literature [14,19–22]. As discussed previously [23], this contraction could be caused by the possible charge compensation mechanisms as the Gd content increases; (i) the creation of the smaller U^V cation; and (ii) the formation of O_V [5,12,14]. There is evidence that both mechanisms may be operative. For the

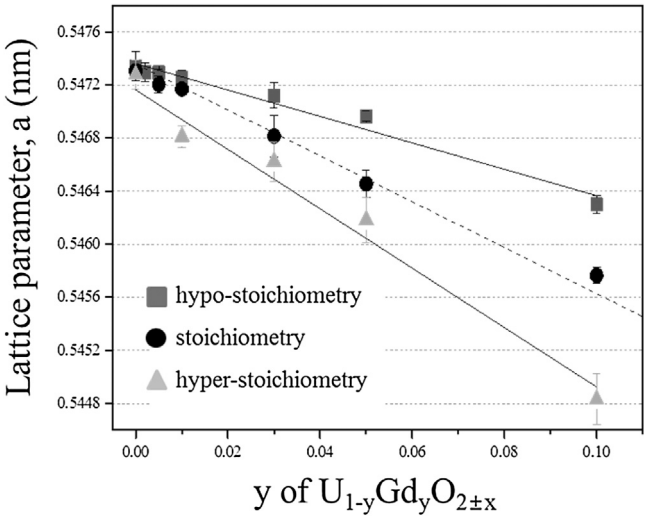

Fig. 1. Lattice parameters for hypostoichiometric $U_{1-y}Gd_yO_{2-x}$, hyperstoichiometric $U_{1-y}Gd_yO_{2+x}$ and stoichiometric $U_{1-y}Gd_yO_2$ as a function of the molar fraction of Gd (y). The dashed line shows the theoretical lattice parameter with Gd content for the perfect stoichiometric $U_{1-y}Gd_yO_2$, where x = 0.

hyperstoichiometric $U_{1-y}Gd_yO_{2+x}$, the contraction factor (the slope of the relationship between the lattice parameter and the Gd content (y)) in Fig. 1 is considerably higher. For relatively small degrees of hyperstoichiometry (up to x = 0.05), when the oxide retains a random defect structure, a contraction of the lattice is expected due to the accommodation of interstitial oxygen (O_I) ions and the creation of the considerably smaller cation (U^V (0.86 Å)) compared to U^{IV} (1.05 Å) [24,25]. By contrast, the lattice parameter for hypostoichiometric $U_{1-y}Gd_yO_{2-x}$ changes more gradually with Gd content, Fig. 1 (slope = −0.00995). According to Ohmichi et al. [14], this can be attributed to the presence of a higher concentration of O_Vs which are ~10% larger than the O^{II} ion (1.24 Å). This partially compensates for the lattice contraction enforced by the increasing Gd^{III} content.

For the more heavily Gd-doped hyperstoichiometric (5 and 10 mol%) $U_{1-y}Gd_yO_{2+x}$ specimens, somewhat larger standard

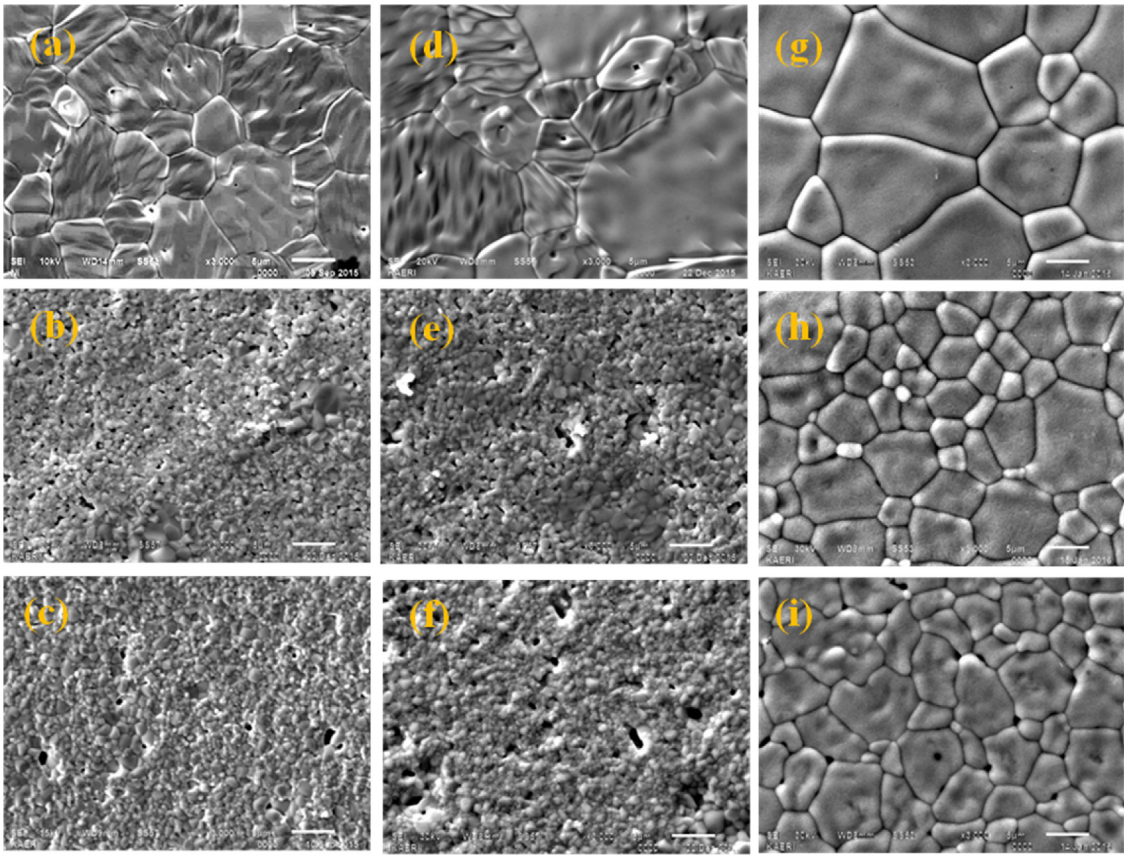

Fig. 2. SEM micrographs for (a-c) hypostoichiometric $U_{1-y}Gd_yO_{2-x}$, (d-f) stoichiometric $U_{1-y}Gd_yO_2$ and (g-i) hyperstoichiometric $U_{1-y}Gd_yO_{2+x}$ for different Gd contents: (a, d, g) y = 0, (b, e, h) y = 0.05, and (c, f, i) y = 0.10. The scale bar is 5 μm.

deviations in lattice parameter are observed compared to the hypostoichiometric specimens as indicated in Fig. 1. This may reflect a slight non-homogeneity of Gd distribution in these pellets.

In hyperstoichiometric $U_{1-y}Gd_yO_{2+x}$

$$\alpha\ (\text{nm}) = 0.5472\ (\pm 0.0001) - \mathbf{0.0233}\ (\pm 0.0026) \times y \quad R^2 = 0.975 \quad \text{(Eq. 1)}$$

In hypostoichiometric $U_{1-y}Gd_yO_{2-x}$,

$$\alpha\ (\text{nm}) = 0.5473\ (\pm 0.0001) - \mathbf{0.0099}\ (\pm 0.0009) \times y \quad R^2 = 0.968 \quad \text{(Eq. 2)}$$

3.2. Surface Morphology

Besides influencing the lattice parameter, Gd has a significant effect on grain growth during sintering. When sintered at 1700 °C in H_2 for 18 hours to produce hypostoichiometry, the pellets exhibited a weight decrease and the grain structure changed markedly with Gd content. The undoped, hypostoichiometric UO_{2-x} exhibited polygonal wrinkled grains with 5 ~ 15 μm in size, Fig. 2(a). The grain size decreases drastically as the Gd content increases, Fig. 2(b) and (c), a feature possibly attributed to the contraction of the fluorite lattice leading to a suppression of U atom diffusion [26,27].

Stoichiometric pellets sintered with CO/CO_2 gas mixtures exhibited large grains (over 20 μm in size), Fig. 2(d). The grain size decreased with increased Gd content, with small grains and intergranular pores developing at high doping levels.

The morphology of hyper-stoichiometric UO_{2+x} consists of large grains (over 20 μm in size) with smooth surfaces, Fig. 2(g). The O_I ions present induce internal strain which distorts the cubic lattice resulting in enhanced U diffusion and crystal growth [27]. Similar smooth surface morphologies have been observed previously for hyperstoichiometric UO_{2+x} [3]. As for hypostoichiometric and stoichiometric specimens, the addition of Gd leads to a decrease in grain size, but to a much larger extent. While the number of O_V will be lower for hyperstoichiometric UO_{2+x}, the presence of O_I leads to the formation of defect clusters involving the association of O_V, O_I and U^V states, and the introduction of transport pathways which facilitate U transport despite the influence of Gd doping.

3.3. Electrical Conductivity

Fig. 3 shows the electrical conductivity for hypostoichiometric, stoichiometric and hyperstoichiometric specimens as a function of Gd-content. Stoichiometric UO_2 is well characterized as a Mott-Hubbard insulator. Fig. 3 shows the conductivity of stoichiometric UO_2 initially increased linearly with Gd content, as previously observed by Kubo et al. [28]. At higher Gd contents, the conductivity became independent of Gd-content and possibly decreased slightly at the highest doping level. A possible explanation is that this independence is attributable to the very small grain size. Using impedance measurements, it has been proposed that there are two conductivity pathways, matrix and grain boundary, both attributed to the creation of U^V ions leading to holes in the U5f level. These holes migrate by a polaron hopping process in which the normally localized electrons are transported between cations by a series of thermally-assisted jumps [29,30]. Matrix conductivity was found to increase linearly with increased doping while grain boundary conductivity initially increased but then decreased. This decrease was attributed to segregation of Gd to the grain boundaries leading to the formation of a Schottky barrier against the migration of holes. Such a segregation process would also limit the increase in matrix conductivity as the overall Gd content increased, and could also contribute to the limited grain growth observed. A combination of these conflicting effects on conductivity could account for the overall insensitivity of the conductivity to Gd content observed for stoichiometric $U_{1-y}Gd_yO_2$ at high doping levels.

For hypostoichiometric $U_{1-y}Gd_yO_{2-x}$, the conductivity exhibits a similar trend with increasing Gd content although the overall values are slightly lower. For hyperstoichiometric $U_{1-y}Gd_yO_{2+x}$, the conductivity increases with Gd content, suggesting that the influence of Gd on the matrix conductivity (i.e., the creation of holes in the U5f level) is dominant and not counterbalanced by the formation of grain boundary Schottky barriers, as indicated by the enhanced grain growth in $U_{1-y}Gd_yO_{2+x}$ compared to the other two specimens (Fig. 2).

3.4. Electrochemical Behaviour

Fig. 4 shows CVs recorded on the hypostoichiometric, stoichiometric and hyperstoichiometric specimens in 0.1 M NaCl

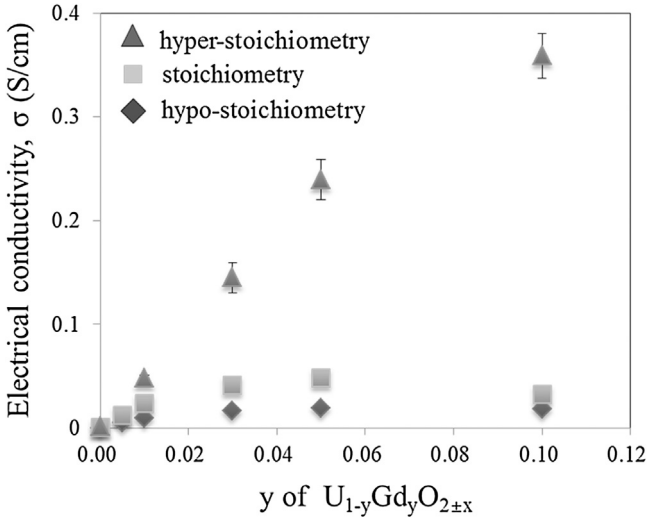

Fig. 3. Electrical conductivity of hyperstoichiometric $U_{1-y}Gd_yO_{2+x}$, hypostoichiometric $U_{1-y}Gd_yO_{2-x}$, and stoichiometric $U_{1-y}Gd_yO_2$ pellets as a function of Gd content.

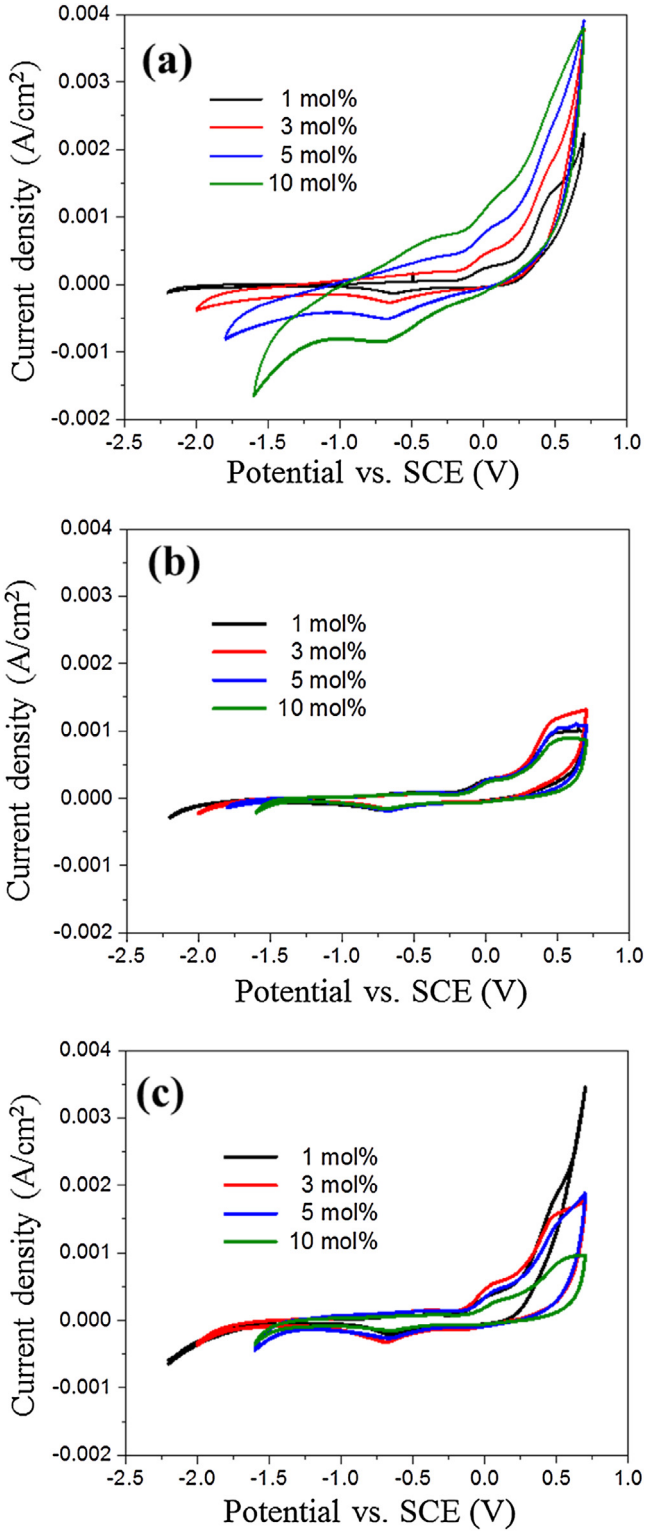

Fig. 4. Cyclic voltammograms recorded on (a) hypostoichiometric $U_{1-y}Gd_yO_{2-x}$, (b) stoichiometric $U_{1-y}Gd_yO_2$ and (c) hyperstoichiometric $U_{1-y}Gd_yO_{2+x}$ electrodes in a 0.1 M NaCl solution containing 0.01 M CO_3^{2-}/HCO^- at pH 8.9, respectively. Scan rate was 50 mV/s.

containing 0.01 M CO_3^{2-}/HCO_3^- (at pH = 8.9). In all three cases the CVs have the features expected for the voltammetric behaviour of UO_2. In the potential range −0.2 V to *c.a.* 0.2 V (region 1), the current can be attributed to the injection of O_I ions leading to the formation of a thin U^{IV}/U^V surface layer ($U^{IV}_{1-2x}U^V_{2x}O_{2+x}$ for undoped UO_2). At higher potentials (region 2), the current increase can be attributed to the further oxidation of this layer to U^{VI} which dissolves in to solution as $U^{VI}O_2(CO_3)_2^{2-}$ in HCO_3^-/CO_3^{2-} solution. The tendency of the current to become independent of potential at very positive values is due to the formation of a thin surface layer of $U^{VI}O_2CO_3$, whose dissolution becomes chemically controlled by further complexation to produce the soluble species. On the reverse cathodic voltammetric scan, the shallow broad peak at around −0.7 V has been shown to be due to the partial reduction of

the oxidized surface layers (in particular the $U^{IV}_{1-2x}U^{V}_{2x}O_{2+x}$) layer [31,32].

For the stoichiometric specimens, Fig. 4(b), there is no discernible influence of Gd-doping on the formation of the surface $U^{IV}_{1-2x}U^{V}_{2x}O_{2+x}$ layer (region 1), as previously observed [23]. However, the anodic oxidation of this layer to U^{VI} (as either dissolved $U^{VI}O_2(CO_3)_2^{2-}$ or a surface layer of $U^{VI}O_2CO_3$) (region 2) shows a slight increase in current followed by a decrease at higher Gd contents (y = 0.05 and 0.10). As described previously, this can be attributed to a competition between conflicting effects. For low Gd^{III} contents, the current increase reflects the increase in O_V caused by doping leading to an increase in the anodic oxidation rate, while at higher doping levels, the observed contraction of the UO_2 lattice and the elimination of O_V due to the formation of Gd^{III}-O_V clusters enforce a decrease in rate. The effect of these competing influences is that the overall influence of Gd-doping is minor.

For hypostoichiometric $U_{1-y}Gd_yO_{2-x}$, the anodic reactivity is strongly enhanced compared to the stoichiometric specimens. This is clear from the CVs shown in Fig. 4(a), despite both the capacitive charging observed and the strong enhancement of H_2O oxidation and reduction at the anodic and cathodic potential limits. At the lowest Gd doping level (y = 0.01), the two oxidation stages ($U^{IV}O_2 \rightarrow U^{IV}_{1-2x}U^{V}_{2x}O_{2+x}$ and $U^{IV}_{1-2x}U^{VI}_{2x}O_{2+2x} \rightarrow U^{VI}O_2CO_3$ and $U^{VI}O_2(CO_3)_2^{2-}$) are distinct and occur in the same potential ranges as observed for the stoichiometric specimens. Although superimposed on the increasing current due to H_2O oxidation to O_2, the current for the second stage of anodic oxidation appears to be enhanced. According to Park and Olander [11] the dominant defects in Gd-doped hypostoichiometric UO_2 are the Gd^{III}-O_V clusters and O_V. While it is difficult to determine whether an increase in Gd-doping increases the anodic reactivity of the UO_2 matrix at positive potentials, it is clear that oxidation is enhanced at lower potentials (~−0.7 V to −0.2 V, Fig. 4(a)). Oxidation in this potential region is sub-thermodynamic and its occurrence may reflect (i) the increased O_V content of the hypostoichiometric UO_2; (ii) the decreased contraction of the lattice for $U_{1-y}Gd_yO_{2-x}$ compared to $U_{1-y}Gd_yO_2$ observed by XRD (Fig. 1), which would be expected to enhance the incorporation of oxygen into available interstitial sites; and (iii) the presence of a high density of more reactive grain boundaries.

For hyperstoichiometric $U_{1-y}Gd_yO_{2+x}$, Fig. 4(c), the highest reactivity is observed for the least Gd-doped specimen, as observed previously [1,4], and attributed to the formation of U-O_V clusters which enhance O_I mobility in the matrix, allowing surface oxidation to penetrate to slightly deeper locations. For small degrees of non-stoichiometry, this leads to a minor contraction of the fluorite lattice [25]. As the Gd content is increased, the electrochemical reactivity for both stages of anodic oxidation decreases, Fig. 4(c), with currents at the highest doping level decreased to values very similar to those observed for the similarly doped stoichiometric specimens, Fig. 4(b). This loss of reactivity with increased Gd content can be attributed to the elimination of available O_V due to Gd^{III}-O_V clustering, which leads to a significant lattice contraction as shown in Fig. 1, any enhanced reactivity due to hyperstoichiometry being rapidly overwhelmed. Since the electrochemical currents observed for the highly Gd-doped (y = 0.10) stoichiometric and hyperstoichiometric specimens are effectively the same, any influence of grain structure, which is very different for the two sets of specimens (Fig. 2) appears minimal.

4. Conclusions

The influence of Gd-doping on the structural and electrochemical properties has been investigated for hypostoichiometric $U_{1-y}Gd_yO_{2-x}$, stoichiometric $U_{1-y}Gd_yO_2$ and hyperstoichiometric $U_{1-y}Gd_yO_{2+x}$. In all cases doping leads to a lattice contraction with the contraction factor increasing in the order

$$U_{1-y}Gd_yO_{2-x} < U_{1-y}Gd_yO_2 < U_{1-y}Gd_yO_{2+x}$$

For the hypostoichiometric and stoichiometric specimens, the grain size decreased markedly with increased Gd doping level, possibly due to the suppression of U atom diffusion as a consequence of the lattice contraction. For the hyperstoichiometric specimen, the decrease in grain size was minor, possibly due to the introduction of transport pathways which facilitate U diffusion.

The electrical conductivity of the hypostoichiometric and stoichiometric specimens changed only slightly with increased Gd content, possibly due to the formation of Schottky barriers caused by Gd accumulation at grain boundaries. For the hyperstoichiometric specimen, the conductivity increased linearly with Gd content, indicating the influence of Gd doping was dominant.

For stoichiometric $U_{1-y}Gd_yO_2$, the overall influence of Gd-doping on electrochemical reactivity was minor, the increase at low doping levels due to an increase in O_V content being counterbalanced at higher doping levels by lattice contraction and Gd^{III}-O_V clustering. For hypostoichiometric $U_{1-y}Gd_yO_{2-x}$, the reactivity increases with Gd content. This may be due to an increase in O_V content and a smaller lattice contraction with increasing doping level. For hyperstoichiometric $U_{1-y}Gd_yO_{2+x}$, the high reactivity at low Gd levels can be attributed to the formation of the U-O_V clusters associated with excess oxygen. The anodic reactivity decreased as the Gd level increased due to the elimination of O_V by Gd^{III}-O_V clustering.

Acknowledgment

This work supported by the National Research Foundation of Korea (NRF) grant funded by the Korea government (MSIP) (No. 2017M2A8A5014754).

References

[1] D.W. Shoesmith, The chemistry/electrochemistry of spent nuclear fuel as a wasteform, in: P. Burns, G. Simon (Eds.), Uranium: Cradle to Grave, vol. 43, Mineralogical Society of Canada, Short Course Series, 2013 Ch. 11 p. 337..
[2] H. He, M. Broczkowski, K. O'Neil, D. Ofori, O. Semenikhin, D. Shoesmith, Corrosion of nuclear fuel (UO_2) inside a failed nuclear waste container, Report NWMO TR-2012-09, Nuclear Waste Management Organization, Toronto, ON, 2012.
[3] H. He, Z. Qin, D.W. Shoesmith, Characterizing the relationship between hyperstoichiometry, defect structure and local corrosion kinetics of uranium dioxide, Electrochim. Acta 56 (2010) 53.
[4] H. He, R.K. Zhu, Z. Qin, P. Keech, Z. Ding, D.W. Shoesmith, Determination of local corrosion kinetics on hyper-stoichiometric UO_{2+x} by scanning electrochemical microscopy, J. Electrochem. Soc. 156 (2009) C87.
[5] H. He, P.G. Keech, M.E. Broczkowski, J.J. Noel, D.W. Shoesmith, Characterization of the influence of fission product doping on the anodic reactivity of uranium dioxide, Can. J. Chem. 85 (2007) 702.
[6] J.M. Konings, T. Wiss, O. Benes, Predicting material release during a nuclear reactor accident, Nat. Mater. 14 (2015) 247.
[7] A.C. Fraker, Corrosion of zircaloy spent fuel cladding in a repository NIST Report: NISTIR 89-4114, 1989.
[8] R.J. McEachern, D.C. Doern, D.D. Wood, The effect of rare-earth fission products on the rate of U_3O_8 formation on UO_2, J. Nucl. Mater. 252 (1998) 145.
[9] L.E. Thomas, R.E. Einziger, H.C. Buchanan, Effect of fission products on air-oxidation of LWR spent fuel, J. Nucl. Mater. 201 (1993) 310.
[10] S.M. Ho, K.C. Radford, Structural chemistry of solid solutions in the UO_2-Gd_2O_3 systems, Nucl. Techn. 73 (1986) 350.
[11] K. Park, D.R. Olander, Defect models for the oxygen potentials of gadolinium and europium-doped Urania, J. Nucl. Mater. 187 (1992) 89.
[12] H.G. Riella, M. Durazzo, M. Hirata, R.A. Nogueira, UO_2-Gd_2O_3 solid solution formation from wet and dry processes, J. Nucl. Mater. 178 (1991) 204.
[13] T.B. Lindemer, A.L. Sutton Jr., Study of nonstoichiometry of $<U_{1-z}Gd_zO_{2\pm x}>$, J. Am. Ceram. Soc. 71 (1988) 553.
[14] T. Ohmichi, S. Fukushima, A. Maeda, H. Watanabe, On the relation between lattice parameter and O/M ratio for uranium dioxide-trivalent rare earth oxide solid solution, J. Nucl. Mat. 102 (1981) 40.

[15] M. Razdan, D.W. Shoesmith, The electrochemical reactivity of 6.0 wt% Gd-doped UO_2 in aqueous carbonate/bicarbonate solutions, J. Electrochem. Soc. 161 (2014) H225.
[16] M. Razdan, D.W. Shoesmith, Influence of trivalent-dopants on the structural and electrochemical properties of uranium dioxide (UO_2), J. Electrochem. Soc. 161 (2014) H105.
[17] J. Lee, J. Kim, Y.-S. Youn, N. Liu, J.-G. Kim, Y.-K. Ha, D.W. Shoesmith, J.-Y. Kim, Raman study on structure of U1-y GdyO2-x (y = 0.005, 0.01, 0.03, 0.05 and 0.1) solid solutions, J. Nucl. Mater. 486 (2017) 216.
[18] L. Desgranges, Y. Pontillon, P. Matheron, M. Marcet, P. Simon, G. Guimbretière, F. Porcher, Miscibility gap in the U–Nd–O phase diagram: a new approach of nuclear oxides in the environment? Inorg. Chem. 51 (2012) 9147.
[19] A.G. Leyva, D. Vega, V. Trimarco, D. Marchi, Homogeneity characterisation of sintered (U,Gd)O_2 pellets by X-ray diffraction, J. Nucl. Mater. 303 (2002) 29.
[20] M. Hirai, S. Ishimoto, Thermal diffusivities and thermal conductivities of UO_2-Gd_2O_3, J. Nucl. Sci. Technol. 28 (1991) 995.
[21] M. Durazzo, F.B.V. Oliveira, E.F.U. de Carvalho, H.G. Riella, Phase studies in the UO_2-Gd_2O_3 system, J. Nucl. Mater. 400 (2010) 183.
[22] T. Cardinaels, J. Hertog, B. Vos, L. de Tollenaere, C. Delafoy, M. Verwerft, Dopant solubility and lattice contraction in gadolinia and gadolinia–chromia doped UO_2 fuels, J. Nucl. Mater. 424 (2012) 289.
[23] N. Liu, J. Kim, J. Lee, Y. Youn, J.-G. Kim, J.-Y. Kim, J.J. Noël, D.W. Shoesmith, Influence of Gd doping on the structure and electrochemical reactivity of UO_2, submitted as a back-to-back article with our current manuscript to Electrochimica Acta.
[24] H. He, D. Shoesmith, Raman spectroscopic studies of defect structures and phase transition in hyper-stoichiometric UO_{2+x}, Phys. Chem. Chem. Phy. 12 (2010) 8108.
[25] K. Teske, H. Ullmann, D. Reytig, Investigation of the oxygen activity of oxide fuels and fuel-fission product systems by solid electrolyte techniques. Part 1: Qualification and limitations of the method, J. Nucl. Mater. 116 (1983) 260.
[26] J.E. Littlechild, G.G. Butler, G.W. Lester, The production of burnable poison oxide fuel, Proc. Int. Conf. BNES on Nuclear Fuel Performance, London, UK, 15-19 October, 1973 p.65.1.
[27] T. Kogai, R. Iwasaki, M. Hirai, In-pile and out-of-pile grain growth behaviour of sintered UO_2 and (U,Gd)O_2 pellets, J. Nucl. Sci. Techn. 28 (1989) 744.
[28] T. Kubo, S. Ishimoto, T. Koyama, Effects of gadolinium doping on electrical properties of UO_2 grain boundaries, J. Nucl. Sci. Techn. 30 (1993) 664.
[29] T. Ishii, K. Naito, K. Oshima, Electrical conductivity and defect structures in non-stoichiometric UO_{2+x}, J. Nucl. Mater. 36 (1970) 288.
[30] S.-H. Kanga, J.-H. Lee, H.-I. Yoo, H.S. Kim, Y.W. Lee, Non-stoichiometry, electrical conductivity and defect structure of hyper-stoichiometric UO_{2+x}at 1000 °C, J. Nucl. Mater. 277 (2000) 339.
[31] D.W. Shoesmith, Fuel corrosion processes under waste disposal conditions, J. Nucl. Mater. 282 (2000) 1.
[32] B.G. Santos, H.W. Nesbitt, J.J. Noël, D.W. Shoesmith, X-ray photoelectron spectroscopy study of anodically oxidized SIMFUEL surfaces, Electrochim. Acta 49 (2004) 1863.